Positron Emission Tomography Using [^{18}F]Galacto-RGD Identifies the Level of Integrin $\alpha_v\beta_3$ Expression in Man

Ambros J. Beer,[1] Roland Haubner,[9] Mario Sarbia,[2] Michael Goebel,[3] Stephan Luderschmidt,[4] Anca Ligia Grosu,[5] Oliver Schnell,[8] Markus Niemeyer,[6] Horst Kessler,[7] Hans-Jürgen Wester,[1] Wolfgang A. Weber,[10] and Markus Schwaiger[1]

Abstract

Purpose: The integrin $\alpha_v\beta_3$ plays a key role in angiogenesis and tumor cell metastasis and is therefore an important target for new therapeutic and diagnostic strategies. We have developed [^{18}F]Galacto-RGD, a highly $\alpha_v\beta_3$-selective tracer for positron emission tomography (PET). Here, we show, in man, that the intensity of [^{18}F]Galacto-RGD uptake correlates with $\alpha_v\beta_3$ expression.

Experimental Design: Nineteen patients with solid tumors (musculoskeletal system, $n = 10$; melanoma, $n = 4$; head and neck cancer, $n = 2$; gliobastoma, $n = 2$; and breast cancer, $n = 1$) were examined with PET using [^{18}F]Galacto-RGD before surgical removal of the tumor lesions. Snap-frozen specimens ($n = 26$) were collected from representative areas with low and intense standardized uptake values (SUV) of [^{18}F]Galacto-RGD. Immunohistochemistry was done using the $\alpha_v\beta_3$-specific antibody LM609. Intensity of staining (graded on a four-point scale) and the microvessel density of $\alpha_v\beta_3$-positive vessels were determined and correlated with SUV and tumor/blood ratios (T/B).

Results: Two tumors showed no tracer uptake (mean SUV, 0.5 ± 0.1). All other tumors showed tracer accumulation with SUVs ranging from 1.2 to 10.0 (mean, 3.8 ± 2.3; T/B, 3.4 ± 2.2; tumor/muscle ratio, 7.7 ± 5.4). The correlation of SUV and T/B with the intensity of immunohistochemical staining (Spearman's $r = 0.92$; $P < 0.0001$) as well as with the microvessel density (Spearman's $r = 0.84$; $P < 0.0001$) were significant. Immunohistochemistry confirmed lack of $\alpha_v\beta_3$ expression in normal tissue (benign lymph nodes, muscle) and in the two tumors without tracer uptake.

Conclusions: Molecular imaging of $\alpha_v\beta_3$ expression with [^{18}F]Galacto-RGD in humans correlates with $\alpha_v\beta_3$ expression as determined by immunohistochemistry. PET with [^{18}F]Galacto-RGD might therefore be used as a new marker of angiogenesis and for individualized planning of therapeutic strategies with $\alpha_v\beta_3$-targeted drugs.

Personalized medicine with targeted therapies is becoming increasingly important in oncology. Well-known examples of successful applications of drugs specially designed for a specific target include tyrosine kinase inhibitors (Glivec, imatinib, Novartis Pharma, Nuremberg, Germany) in gastrointestinal stroma tumors and chronic myeloid leukemia or Herceptin (Trastuzumab, Genentech, South San Francisco, CA), which targets the HER-2/*neu* receptor, in breast cancer (1, 2). The integrin $\alpha_v\beta_3$ is another interesting target for specific therapies in oncology, as it is highly expressed on activated endothelial cells during angiogenesis and plays an important role in the regulation of tumor growth, local invasiveness, and metastatic potential (3, 4). Therapeutic strategies include the use of humanized antibodies directed against $\alpha_v\beta_3$ (Vitaxin, MedImmune, Gaithersburg, MD) or cyclic pentapeptides with specific binding to $\alpha_v\beta_3$ (Cilengitide, EMD 121974, Merck Pharma GmbH, Darmstadt, Germany), which are currently evaluated in phase I and II studies (5, 6). A well-known disadvantage is that, in many cases, the expression of highly specific targets is limited to a subset of patients. In breast cancer, for example, only 30% of tumors overexpress HER-2/*neu*, and only these patients will profit from a Herceptin therapy (7). The same might be true for $\alpha_v\beta_3$ because its expression depends on tumor type and tumor stage. It has been shown for human melanoma, for example, that the expression of $\alpha_v\beta_3$ plays an important role during the transition of cells from the radial growth phase to the vertical growth phase (8). However, further changes leading to metastases may be more complex and not ultimately dependent on $\alpha_v\beta_3$ expression (9). Hence, a strategy to assess the intensity of $\alpha_v\beta_3$ expression noninvasively in

Authors' Affiliations: Departments of [1]Nuclear Medicine, [2]Pathology, [3]Orthopedic Surgery, [4]Dermatology, [5]Radiation Therapy, and [6]Gynecology and [7]Department Chemie, Lehrstuhl II für Organische Chemie, Technische Universität München; [8]Department of Neurosurgery, Ludwig Maximilians Universität München, Munich, Germany; [9]Universitätsklinik für Nuklearmedizin, Medizinische Universität Innsbruck, Innsbruck, Austria; and [10]Department of Molecular and Medical Pharmacology, David Geffen School of Medicine, University of California, Los Angeles, California

Received 2/6/06; revised 4/7/06; accepted 4/28/06.

Grant support: Münchner Medizinische Wochenschrift and Sander Foundation.

The costs of publication of this article were defrayed in part by the payment of page charges. This article must therefore be hereby marked *advertisement* in accordance with 18 U.S.C. Section 1734 solely to indicate this fact.

Requests for reprints: Ambros J. Beer, Klinikum rechts der Isar, Department of Nuclear Medicine, Technische Universität München, Ismaninger Strasse 22, 81675 Munich, Germany. Phone: 49-89-4140-2971; Fax: 49-89-4140-4841; E-mail: beer@roe.med.tum.de.

doi:10.1158/1078-0432.CCR-06-0266

humans would be of paramount importance for the selection of those patients most amenable to $\alpha_v\beta_3$-targeted therapies. Therefore, we have developed the tracer [^{18}F]Galacto-RGD for positron emission tomography (PET). [^{18}F]Galacto-RGD showed high affinity and selectivity for the $\alpha_v\beta_3$ integrin *in vitro*, receptor-specific accumulation in a murine $\alpha_v\beta_3$-positive tumor model, as well as high metabolic stability and predominantly renal elimination (10). Moreover, initial data from our patient study indicate that this tracer can be successfully used to image $\alpha_v\beta_3$-positive tumors with good contrast (11, 12). The purpose of this study was to correlate the uptake of [^{18}F]Galacto-RGD with *ex vivo*-determined intensity of $\alpha_v\beta_3$ expression to prove that PET using [^{18}F]Galacto-RGD correctly identifies the level of $\alpha_v\beta_3$ expression in man.

Materials and Methods

Radiopharmaceutical preparation. Synthesis of the labeling precursor and subsequent ^{18}F labeling were carried out as described previously (11).

Patients. The study was approved by the ethics committee of the Technische Universität München (Munich, Germany), and informed written consent was obtained from all patients. Nineteen consecutive patients were included in the study and examined between February 2004 and March 2005 (11 female and 8 male; age, 55.9 ± 16.7 years; range, 31-84 years). Inclusion criteria consisted of known or suspected solid malignancy scheduled for surgery with a size >1 cm in maximum diameter as determined by magnetic resonance imaging (MRI) or computed tomography, age >18 years, and the ability to give written and informed consent. Exclusion criteria consisted of pregnancy, lactation period, time interval between PET scan and operation of >2 weeks (to obtain tissue within a narrow time frame), and impaired renal function (serum creatinine level, >1.2 mg/dl).

PET imaging procedure. Imaging was done with an ECAT EXACT PET scanner (CTI/Siemens, Knoxville, TN). Before injection of [^{18}F]Galacto-RGD (133-200 MBq), a transmission scan was acquired for 5 minutes per bed position (five bed positions) using three rotating ^{68}Ge rod sources (each with ~90 MBq ^{68}Ge). In each subject, a static emission scan was acquired in the caudocranial direction, beginning on average 72.0 ± 12.2 minutes after injection of [^{18}F]Galacto-RGD, covering a field of view from the pelvis to the thorax (five to seven bed positions, 5 minutes per bed position). In the four patients with glioblastoma multiforme or head and neck cancer, the head and neck were included in the field of view (two bed positions). When the tumor was located at the extremities (n = 6), the tumor was imaged before the torso (one to two bed positions). The starting time was chosen according to our previous biodistribution studies, which showed rising tumor/blood ratios (T/B) until 1 hour after tracer injection (12).

Image analysis. The tumor size was measured in the preoperative MRI or computed tomography scans, respectively, as the maximum diameter in the plane with the largest tumor extension. The mean tumor size was 6.4 cm (±4.5 cm; range, 1.0-18 cm).

Table 1. Patient data

Patient	Age	Diagnosis	Staining intensity	MVD	SUV	T/B
1	64	Glioblastoma multiforme, periphery	I tumor cells + vessels	2.3	2.2	1.5
		Glioblastoma multiforme, center	0	0	0.5	0.3
2	74	Malignant fibrous histiocytoma	II tumor cells + vessels	7.7	3.2	3.1
		Muscle adjacent to tumor	0	0	0.6	0.6
3	57	Glioblastoma multiforme	I tumor cells + vessels	0.7	1.5	1.7
4	33	SCC oral cavity	I vessels	2.0	3.0	2.5
		Benign lymph node	0	0	0.4	0.3
5	50	lymph node metastasis SCC soft palate	II vessels	3.3	2.9	3.1
6	67	neurinoma	I vessels	1.3	1.5	1.3
7	84	Liposarcoma G1	0	0.7	0.4	0.2
8	66	Melanoma, subcutaneous metastasis	I tumor cells	0	2.2	1.7
		Melanoma, subcutaneous metastasis	I tumor cells	0	2.5	1.9
9	54	Breast cancer	II tumor cells + vessels	2.3	3.1	2.6
10	41	Osteosarcoma	III tumor cells + vessels	3.7	3.3	3.9
11	56	Malignant fibrous histiocytoma	I tumor cells + vessels	1.3	2.9	2.5
12	51	Liposarcoma G1, periphery	I vessels	0.7	1.5	1.1
		Liposarcoma G1, center	0	0	0.3	0.2
13	35	Osteosarcoma, periphery	III tumor cells + vessels	6.7	3.8	3.7
		Osteosarcoma, periphery	III tumor cells + vessels	9	4.0	3.8
14	55	Osseous metastasis (RCC)	II tumor cells + vessels	9	3.0	2.0
15	75	Soft tissue sarcoma	III tumor cells + vessels	31.7	7.0	7.1
		Inflammation	II vessels	3.3	2.0	2.0
16	36	Melanoma, lymph node metastasis	III tumor cells	9	6.0	5.3
17	89	(Melanoma) chronic inflammation	I vessels	4.0	2.3	1.7
18	31	Pigmented villonodular synovitis	III vessels	23.7	3.8	5.4
19	44	Melanoma, lymph node metastasis	III tumor cells	4	4.0	3.6

NOTE: Staining intensity of immunohistochemistry of $\alpha_v\beta_3$ expression.
Abbreviations: SCC, squamous cell carcinoma; RCC, renal cell carcinoma; G, tumor grading.

Positron emission data were reconstructed using the ordered subsets expectation maximization algorithm using eight iterations and four subsets. The images were attenuation corrected using the transmission data collected over the same region of emission imaging. For image analysis, the CAPP software version 7.1 (CTI/Siemens) was used. Images were calibrated to standardized uptake values (SUV; ref. 13). In the static emission scans, circular regions of interest with a diameter of 1.5 cm were placed over the left ventricle (for measurement of blood pool activity), the forearm (for measurement of muscle tissue), and tumor tissue in three adjacent slices by an experienced operator. Results were expressed in mean SUV. Region of interest diameter for tumors was also set to 1.5 cm for lesions >2 cm (n = 24). For two lesions <2 cm (lymph nodes with 15 and 10 mm), the diameter was set to 1 cm to avoid underestimation of the SUV by partial volume effects. Moreover, the maximum SUV measured in this regions of interest was used instead of the mean SUV because the recovery coefficient for lesions with a diameter of 1.5 cm is 70%, assuming a tumor/background ratio of 4 and a spatial resolution of 12 mm according to Brix et al. (14). In the tumors, the areas with the maximum intensity and those regions where the biopsies in the operating room were taken from were chosen for measurements. T/B and tumor/muscle ratios were calculated by the following formulas: SUV_{tumor} / SUV_{blood} and SUV_{tumor} / SUV_{muscle}. All measurements were done before the data from immunohistochemistry were available.

Collection of tissue samples and immunohistochemistry. The mean time interval between PET and operation was 3.5 days. In the operating room, tissue samples from the tumors were obtained from tumor regions with maximum tracer uptake and, when possible, from regions with low tracer uptake. Both the surgeons and a member of the department of nuclear medicine (A.J.B.) were present in the operating room for collection of the tissue samples, and both were aware of the imaging findings of the PET scan, which were shown and discussed the day before the operation. The specimens were snap frozen in liquid nitrogen and stored at −70°C until staining was done.

For immunohistochemical investigation, frozen tumor tissues were sectioned (6 μm) and stained using the biotinylated monoclonal anti-$\alpha_v\beta_3$ antibody LM609 (1:100; Chemicon Europe, Hofheim, Germany). Sections were processed by peroxidase staining (peroxidase substrate kit AEC, Vector Laboratories, Burlingame, CA).

Light microscopic evaluation of the density of $\alpha_v\beta_3$-positive microvessel was done as described previously (15). Briefly, areas with the highest density of $\alpha_v\beta_3$-positive microvessels were identified using scanning magnification. Subsequently, $\alpha_v\beta_3$-positive microvessels were counted in three adjacent microscopic fields using a ×40 magnifying lens and a ×10 ocular, corresponding to an area of 0.588 mm^2.

Staining intensity was determined as described before. The score was calculated similar to the modified histochemical score (H-score; ref. 16). Briefly, the staining positivity was graded on a four-point scale: 0 = no staining, 1 = weak, 2 = moderate, and 3 = strong positivity. The percentage of cells at each intensity was estimated. The score is calculated as 0 × negative % + 1 × weak % + 2 × moderate % + 3 × strongly stained %. The overall staining intensity was then graded in four levels: 0 (score 0-10), I (score 11-100), II (score 101-200,) and III (score 201-300).

Determination of microvessel density (MVD) and staining intensity was done by one senior pathologist (M.S.), who was blinded to the results of the SUV measurements.

Statistical analysis. All quantitative data are expressed as mean ± SD. The correlation between quantitative variables was evaluated by linear regression analysis and calculation of Pearson's correlation coefficient r or by Spearman's rank correlation. Statistical significance was tested by using ANOVA. The correlation between semiquantitative variables and quantitative variables was evaluated by the Spearman's rank correlation. All statistical tests were done at the 5% level of statistical significance using the StatView program (SAS Institute, Inc., Cary, NC) or MedCalc (MedCalc version 6.15.000).

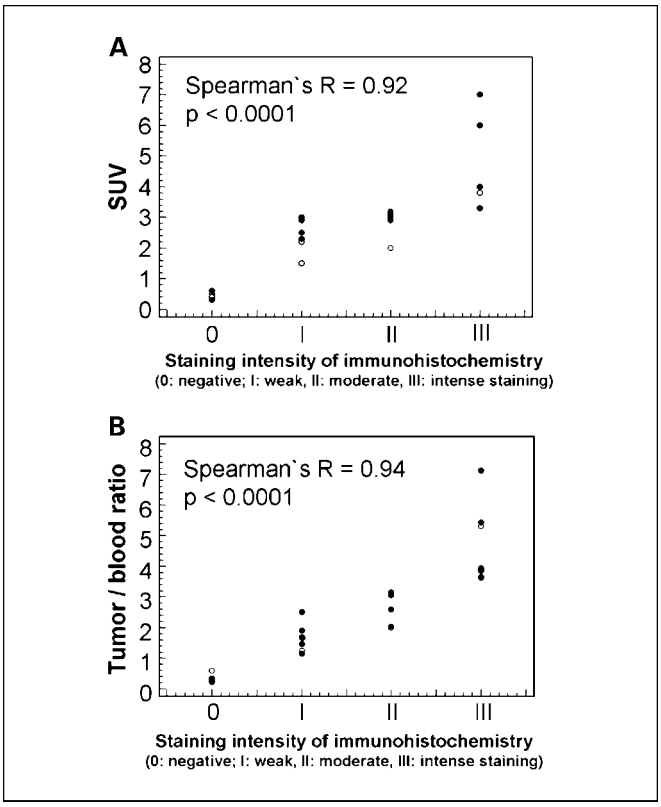

Fig. 1. The correlation between staining intensity of immunohistochemistry and SUVs in the specimens (*A*) and T/B (*B*) determined from [^{18}F]Galacto-RGD PET (●, malignant lesions; ○, benign lesions) are highly significant (Spearman's rank correlation).

Results

Patterns of $\alpha_v\beta_3$ expression and tracer uptake. In 16 of 19 patients, histology confirmed malignant tumors, as suspected by conventional imaging. In three patients with suspected malignancy or inconsistent imaging findings, histology revealed benign tumors. In a patient with melanoma (patient 17), a subcutaneous tumor of the abdominal wall turned out to be a chronic inflammation. In patient 6, histology revealed a neurofibroma in a paravertebral tumor. In patient 18, a tumor of the synovia turned out to be a pigmented villonodular synovitis.

Seventeen of 19 lesions showed tracer accumulation with SUV_{max} ranging from 1.2 to 10.0 (mean, 3.8 ± 2.3; T/B, 3.4 ± 2.2; tumor/muscle ratio, 7.7 ± 5.4). The highest SUVs were found in a soft tissue sarcoma and a lymph node metastasis from melanoma, whereas two low-grade liposarcomas showed no substantial tracer uptake (mean SUV, 0.5 ± 0.1). Immunohistochemical investigation revealed no $\alpha_v\beta_3$ expression in normal tissue and in the two lesions without tracer uptake, whereas all lesions with uptake also showed immunohistochemical $\alpha_v\beta_3$ expression (Table 1). In benign lesions, (pigmented villonodular synovitis, neurofibroma, and inflammatory tissue), $\alpha_v\beta_3$ was located only on the vasculature. In malignant tumors, the patterns of $\alpha_v\beta_3$ expression varied considerably: in lymph node metastasis and cutaneous metastasis from melanoma, $\alpha_v\beta_3$ was predominantly located on the tumor cells. In squamous cell cancer of the head and

neck, $\alpha_v\beta_3$ was located on the neovasculature. In the other tumor entities, $\alpha_v\beta_3$ was located on neovasculature as well as on the tumor cells in varying degrees.

Correlation of tracer uptake and staining intensity of immunohistochemistry. The correlations of SUV and T/B with the intensity of immunohistochemical staining were significant (Figs. 1-3). The correlations were also significant for malignant lesions alone (n = 20; SUV, $P < 0.0001$; T/B, $P < 0.0001$). We also tested if the SUV correlates with the tumor size, but there was no significant correlation (r = 0.14; P = 0.58).

Correlation of tracer uptake and MVD of $\alpha_v\beta_3$-positive vessels. For the correlation of MVD with SUV and T/B, only 22 of 26 specimens were analyzed because, in four specimens, $\alpha_v\beta_3$ expression was present predominantly on tumor cells. Again, the correlations were significant (Figs. 4-6). When all specimens were analyzed (n = 26), the correlations were lower but still significant (SUV, Pearson's r = 0.75; $P < 0.0001$; T/B, Pearson's r = 0.83; $P < 0.0001$).The correlations were also significant for malignant lesions alone (n = 16; SUV, Pearson's r = 0.85; $P < 0.0001$; T/B, Pearson's r = 0.84; $P < 0.0001$). Because two tumors showed an exceptionally high SUV, high T/B and high MVD, we recalculated the linear regression analysis without these two values because they might bias the data. However, the correlation was still significant (SUV, Pearsons's r = 0.79; $P < 0.0001$; T/B, Pearsons's r = 0.72; P = 0.0004).

Discussion

In this study, we have shown that the uptake of the $\alpha_v\beta_3$-selective PET tracer [^{18}F]Galacto-RGD correlates significantly with the staining intensity of immunohistochemistry of $\alpha_v\beta_3$ expression in tumors, as well as with the MVD of $\alpha_v\beta_3$-positive microvessels. We therefore have shown, in man, that PET using [^{18}F]Galacto-RGD correctly identifies the level of $\alpha_v\beta_3$ expression in tissue noninvasively.

Our previous studies with [^{18}F]Galacto-RGD in humans showed the feasibility of using this tracer with good image quality and a favorable biodistribution (11, 12). The findings of this study corroborate our previous findings in a murine tumor model, which showed a linear correlation between α_v integrin expression and [^{18}F]Galacto-RGD uptake (11). There was no correlation between tumor size and [^{18}F]Galacto-RGD uptake, which shows that a higher tracer uptake was not simply caused by a larger tumor volume. Most lesions (n = 24) were >2 cm with a recovery coefficient of >90%, assuming a tumor/background ratio of 4 and a spatial resolution of 12 mm. Therefore, the SUV was not substantially underestimated in the majority of lesions. One small benign lymph node with 10 mm showed no substantial tracer uptake; therefore the recovery coefficient should be ~100% despite the small diameter (14). In one lymph node metastasis with 15 mm and a tumor/background

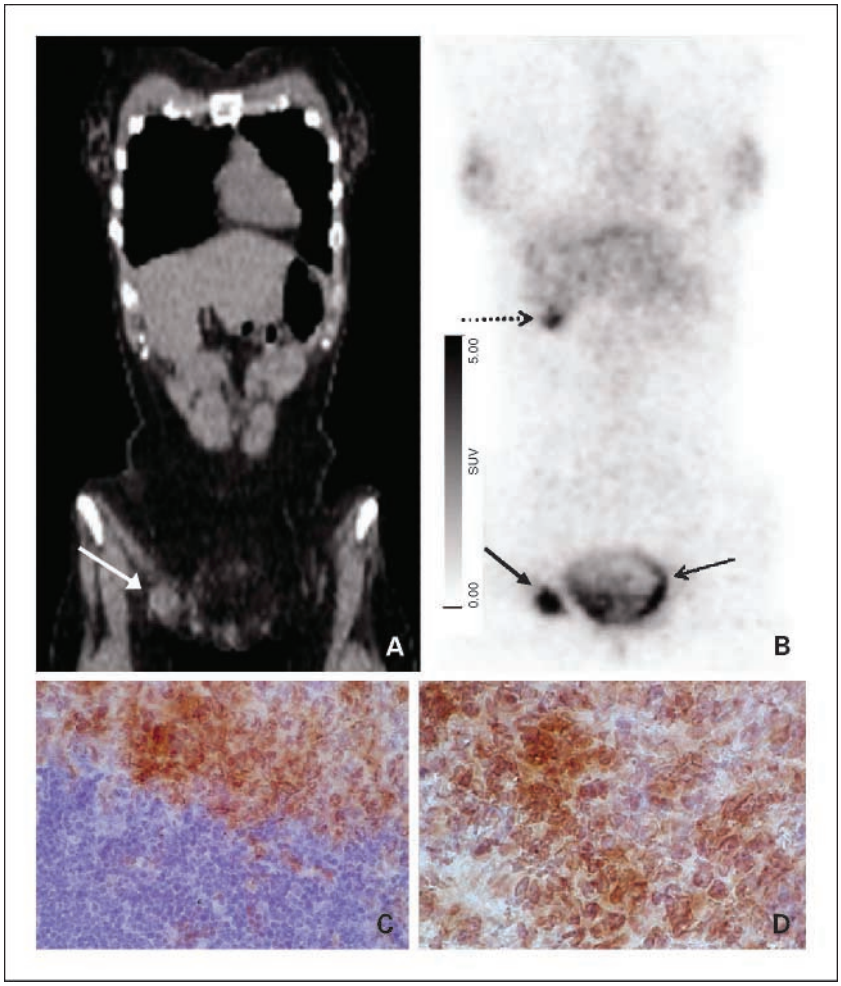

Fig. 2. Female patient (36 years old) with a lymph node metastasis from melanoma. *A,* arrow with closed arrowtip, computed tomography. Note intense [^{18}F]Galacto-RGD uptake (*B*, SUV 6.0; *arrow with open arrowtip*, urinary bladder; *arrow with dotted line*, gall bladder) and intense staining of the tumor cells in immunohistochemistry (*C, top*; *D*, magnification of tumor cells), whereas the normal lymph node tissue is negative (*C, bottom*).

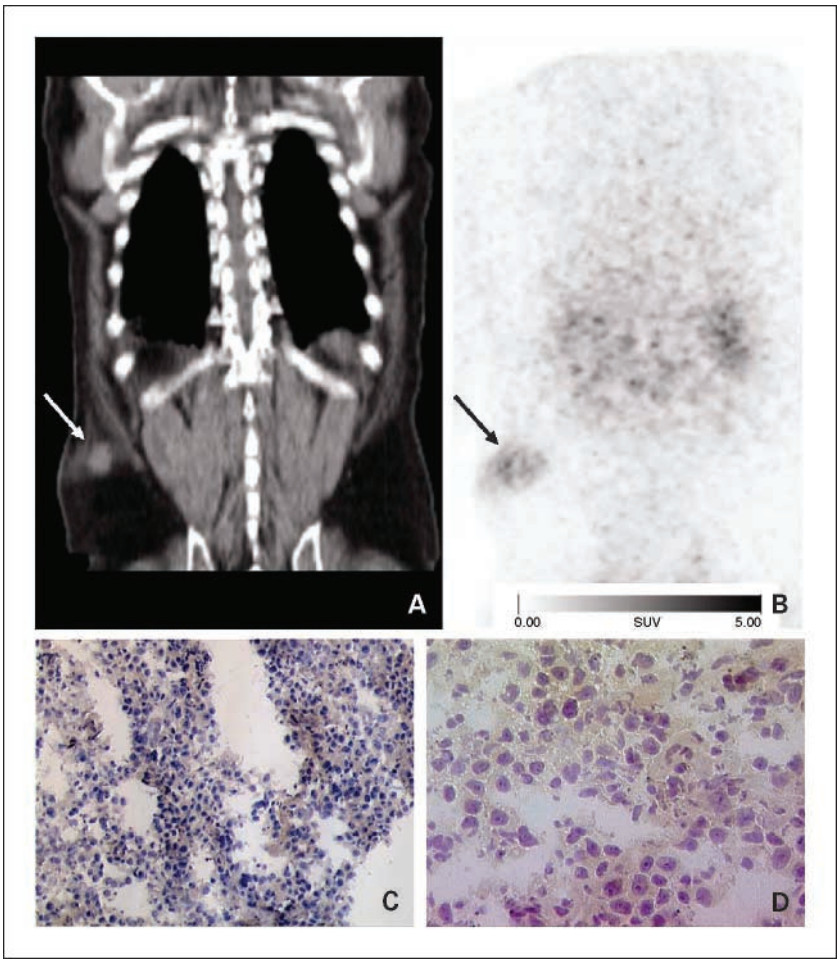

Fig. 3. Male patient (66 years old) with a subcutaneous metastasis from melanoma (*arrow*). *A,* tumor in the right laterodorsal abdominal wall. The tumor shows only moderate [^{18}F]Galacto-RGD uptake (*B*, SUV, 2.2) and only weak staining of the tumor cells in immunohistochemistry (*C* and *D*, magnification of tumor cells).

ratio of 7.8, SUV is probably underestimated by ~30%. The pigmented villonodular synovitis had a maximum diameter of 25 mm, but most parts of the tumor showed a diameter of ≤15 mm. Therefore, in this lesion, the SUV is probably underestimated as well. This might also explain why the SUV in both lesions was not as high, as one might have expected with regard to the intense staining in immunohistochemistry.

Most lesions in this study showed at least some uptake of [^{18}F]Galacto-RGD. This is not surprising because it is known that $\alpha_v\beta_3$ is expressed on angiogenic blood vessels and on malignant tumors at elevated levels (17–19). Therefore, visualization of many tumors should be feasible with an $\alpha_v\beta_3$ imaging agent. However, the diversity of uptake intensity suggests that the intensity of $\alpha_v\beta_3$ expression depends on various factors and is not uniformly high in all tumor entities at all times. The patterns and intensity of $\alpha_v\beta_3$ expression we observed in immunohistochemistry of the tumor specimen confirmed this hypothesis. As expected from literature, $\alpha_v\beta_3$ expression could be documented in varying degrees on the neovasculature of malignant as well as benign tumors or inflammatory processes (20, 21). The MVD of $\alpha_v\beta_3$-positive vessels correlated significantly with the uptake of [^{18}F]Galacto-RGD. Two lesions showed a substantially higher MVD compared with the other lesions. However, even when these two data points were not considered in the analysis, correlation of MVD and tracer uptake still was highly significant. This underlines the potential of [^{18}F]Galacto-RGD as a new marker of angiogenesis in tumors and in benign processes with elevated levels of angiogenesis. In animal models of chronic inflammation, this has already been shown successfully (22).

Moreover, $\alpha_v\beta_3$ expression was present on cells of malignant tumors in varying intensity, with melanoma cells in lymph node metastases showing the most intense staining. This confirms previously reported results on the importance of $\alpha_v\beta_3$ for the metastatic potential of melanoma cells and their invasion to lymph nodes (9, 23). Well-differentiated tumors, such as low-grade liposarcomas, showed no $\alpha_v\beta_3$ expression in immunohistochemistry and no substantial uptake of [^{18}F]Galacto-RGD, whereas high grade sarcomas showed higher tracer uptake, a higher MVD of $\alpha_v\beta_3$-positive vessels and $\alpha_v\beta_3$-positive tumor cells. The higher degree of $\alpha_v\beta_3$ expression on tumor cells in more aggressive tumors can be explained by the important role of $\alpha_v\beta_3$ in cell migration, invasion, and metastatic activity (24–27). Integrin $\alpha_v\beta_3$ expression has also been reported to be an important prognostic factor in tumors, such as breast and colon cancer (28, 29). Therefore, [^{18}F]Galacto-RGD PET might be a unique tool for noninvasive assessment of the aggressiveness and metastatic potential of a given tumor and, consequently, might be a new prognostic marker.

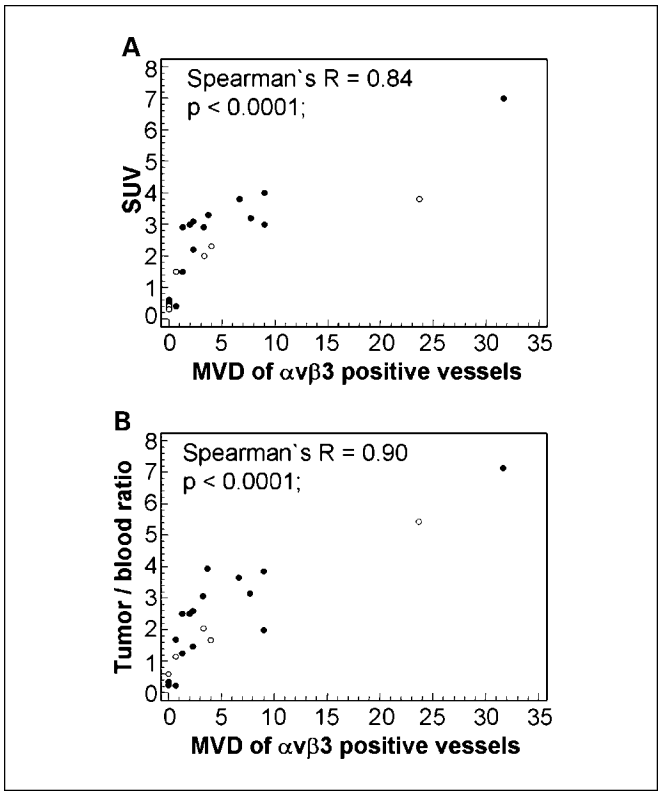

Fig. 4. Spearman's rank correlation of MVD of $\alpha_v\beta_3$-positive vessels in specimens and SUVs (*A*) and T/B (*B*) determined from [^{18}F]Galacto-RGD PET. ●, malignant lesions; ○, empty circles. The correlations are highly significant. Linear regression analysis. *A,* Pearson's $r = 0.81$; *B,* Pearson's $r = 0.87$; *A + B*, $P < 0.0001$.

However, in tumors where $\alpha_v\beta_3$ is predominantly expressed on the tumor cells, [^{18}F]Galacto-RGD is not a pure marker of angiogenesis because the resulting signal combines [^{18}F]Galacto-RGD accumulation in $\alpha_v\beta_3$-expressing neovasculature as well as on $\alpha_v\beta_3$-expressing tumor cells. There was some overlap in MVD notable in the linear regression analysis for SUVs between 2 and 4. This might also be explained by the various amounts of contribution to the PET signal from $\alpha_v\beta_3$ on tumor cells.

About image quality and practicability, tumors with tracer uptake showed excellent tumor/muscle ratios and high T/B. Our previous studies of the kinetics of [^{18}F]Galacto-RGD in tumors showed a plateau of tracer uptake at ~15 minutes after injection and slowly reversible specific tracer binding (12). Therefore, we decided to use simple SUV measurements instead of complex kinetic modeling data for quantitation of uptake. The applied imaging protocol is similar to protocols used for PET with the most widely used tracer [^{18}F]fluorodeoxyglucose and can be transferred easily to a routine clinical setting.

Potential future applications for PET using [^{18}F]Galacto-RGD are manifold. In inflammatory processes, for example, it might be used to assess disease activity noninvasively. It might also be applied for monitoring angiogenesis during antiangiogenic therapies. In this respect, PET has many advantages compared with dynamic contrast-enhanced MRI, which is the modality most commonly applied in clinical studies up to now. Dynamic contrast-enhanced MRI data need to be analyzed using kinetic modeling techniques and are difficult to interpret because dynamic contrast-enhanced MRI represents a complex summation of vascular permeability, blood

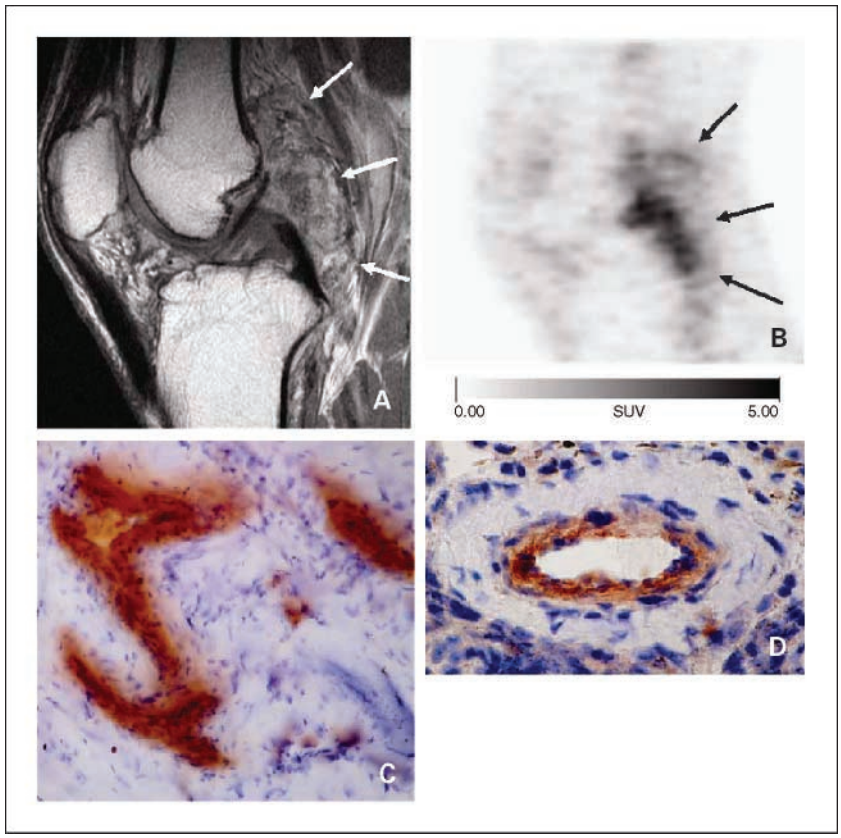

Fig. 5. Male patient (35 years old) with a pigmented villonodular synovitis of the knee (*arrows*). *A,* MRI (sagittal T1-weighed sequence with gadolinium diethylenetriaminepentaacetic acid i.v.) shows the enhancing and thickened synovia. *B,* [^{18}F]Galacto-RGD PET shows moderate to intense uptake of the tumor. SUV, 3.8. *C* and *D,* immunohistochemistry shows intense staining of the neovasculature. *D,* magnification, positive staining of the endothelium of a vessel.

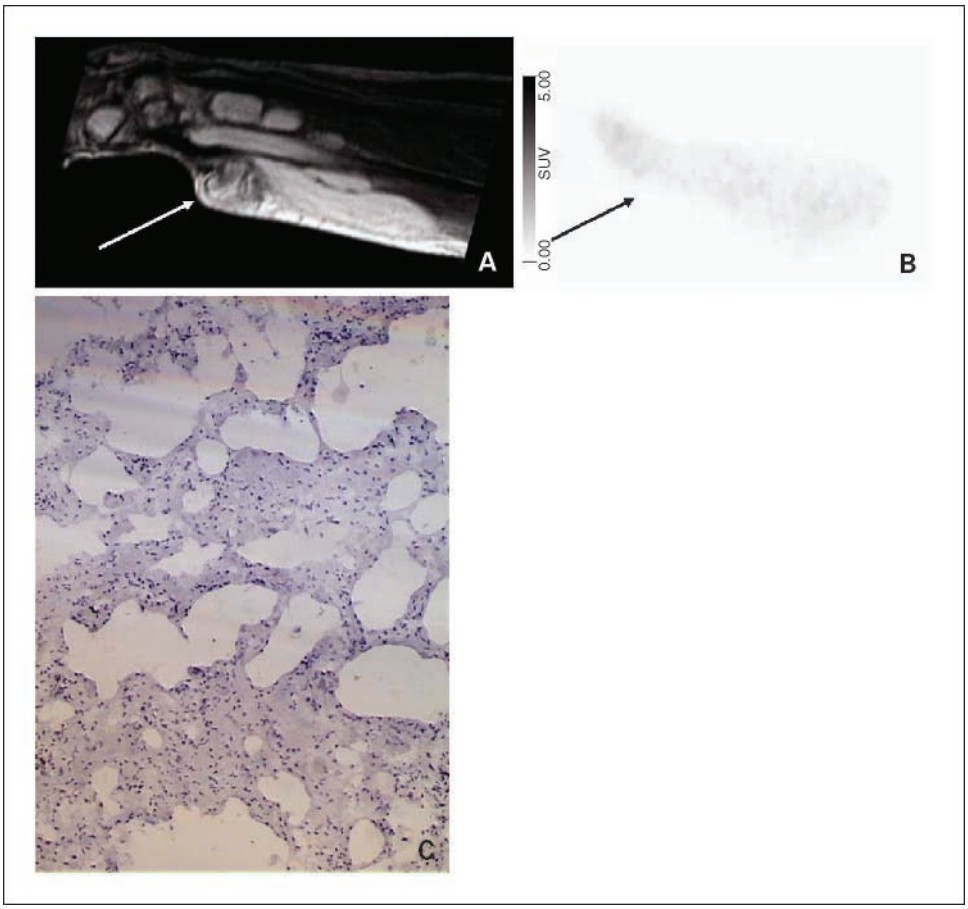

Fig. 6. Female patient (84 years old) with a liposarcoma of the forearm and wrist (*arrow*). *A,* arrow, MRI (T1-weighed sequence with gadolinium diethylenetriaminepentaacetic acid i.v.) shows the fat containing tumor with an enhancing nodule near the wrist. *B,* there is no substantial tumor uptake in [^{18}F]Galacto-RGD PET. SUV 0.4. *C,* immunohistochemistry confirms lack of $\alpha_v\beta_3$ expression.

flow, vascular surface area, and interstitial pressure (30). The approach of targeting the $\alpha_v\beta_3$ integrin on the other hand is very specific. Moreover, only a limited part of the body can be examined with dynamic contrast-enhanced MRI, whereas with PET tracer uptake can be analyzed in the whole body.

Finally, a promising application of [^{18}F]Galacto-RGD PET would be the determination of the $\alpha_v\beta_3$ receptor status before starting therapies targeted against $\alpha_v\beta_3$, such as with Vitaxin or Cilengitide (5, 31). As $\alpha_v\beta_3$ expression is very heterogeneous depending on tumor type and stage, this would be of paramount importance because patients with low levels of $\alpha_v\beta_3$ expression could switch to an alternative regimen in the first place, avoiding ineffective treatment.

There are potential limitations to our study. We had to work with snap-frozen specimen because there is currently no $\alpha_v\beta_3$ antibody available, which works on paraffin-embedded specimen. This limited the number and size of the specimen we could obtain per tumor. The quality of snap-frozen specimen also is inferior to paraffin-embedded material. Moreover, the spatial resolution of PET is limited; therefore, the exact area, where the tissue sample was taken from, can only be estimated. Therefore, we cannot exclude that due to the heterogeneity of some tumors, there might have been areas with higher MVD, resulting in false low vessel counts and vice versa. The use of immunohistochemistry also allows only for a semiquantitative analysis of $\alpha_v\beta_3$ expression. No quantitative protein measurements were done because, currently, no Western blot technique for the combined $\alpha_v\beta_3$ integrin subunits is available. However, we think that for most future applications of [^{18}F]Galacto-RGD PET in patients, a semiquantitative assessment of $\alpha_v\beta_3$ expression would be sufficient, similar for example to the semiquantitative analysis of HER-2/*neu* expression with immunohistochemistry in breast cancer by the DAKO score before starting Herceptin therapy (32). Moreover, for an exact quantification of receptor density in PET, dynamic scans with arterial blood sampling would probably have to be done over the tumor area in addition to static emission scans, limiting the use of [^{18}F]Galacto-RGD PET in daily routine.

Conclusions

Molecular imaging using PET can effectively show the level of $\alpha_v\beta_3$ expression in man. Therefore, a new imaging tool for assessment of angiogenesis and the metastatic potential of tumors is at hand. Future studies will focus on its use as a tool for planning and controlling $\alpha_v\beta_3$-targeted therapies and as a prognostic marker.

Acknowledgments

We thank Wolfgang Linke, Janette Carlsen, Christa Schott, Karl Friedrich Becker, and the RDS-Cyclotron and PET team, particularly Michael Herz, Petra Watzlowick, Gitti Dzewas, Coletta Kruschke, and Nicola Henke for excellent technical assistance.

References

1. Krause DS, Van Etten RA. Tyrosine kinases as targets for cancer therapy. N Engl J Med 2005;353:172–87.
2. Gasparini G, Longo R, Torino F, et al. Therapy of breast cancer with molecular targeting agents. Ann Oncol 2005;16:28–36.
3. Hood JD, Cheresh DA. Role of integrins in cell invasion and migration. Nat Rev Cancer 2002;2:91–100.
4. Ruoslahti E. Specialization of tumor vasculature. Nat Rev Cancer 2002;2:83–90.
5. Dechantsreiter MA, Planker E, Mathä B, et al. *N*-methylated cyclic RGD peptides as highly active and selective $\alpha_v\beta_3$ antagonists. J Med Chem 1999;42:3033–40.
6. Patel SR, Jenkins J, Papadopolous N, et al. Pilot study of vitaxin—an angiogenesis inhibitor—in patients with advanced leiomyosarcomas. Cancer 2001;92:1347–8.
7. Zhou BP, Li Y, Hung MC. HER-2/*neu* signalling and therapeutic approaches in breast cancer. Breast Dis 2002;15:13–24.
8. Johnson JP. Cell adhesion molecules in the development and progression of malignant melanoma. Cancer Metastasis Rev 1999;18:345–57.
9. Seftor RE, Seftor EA, Hendrix MJ. Molecular role(s) for integrins in human melanoma invasion. Cancer Metastasis Rev 1999;18:359–75.
10. Haubner R, Wester HJ, Weber WA, et al. Noninvasive imaging of $\alpha(v)\beta3$ integrin expression using ^{18}F-labeled RGD-containing glycopeptide and positron emission tomography. Cancer Res 2001;61:1781–5.
11. Haubner R, Weber WA, Beer AJ, et al. Non-invasive visualization of the activated $\alpha_v\beta_3$ integrin in cancer patients by positron emission tomography and [^{18}F]galacto-RGD. PLoS Medicine 2005;2:e70.
12. Beer AJ, Haubner R, Goebel M, et al. Biodistribution and pharmacokinetics of the $\alpha_v\beta_3$ selective tracer ^{18}F galacto-RGD in cancer patients. J Nucl Med 2005;46:1333–41.
13. Weber WA, Ziegler SI, Thodtman R, et al. Reproducibility of metabolic measurements in malignant tumors using FDG PET. J Nucl Med 1999;40:1771–7.
14. Brix G, Bellemann ME, Hauser H, Doll J. Recovery coefficients for the quantification of the arterial input functions from dynamic PET measurements: experimental and theoretical determination. Nuklearmedizin 2002;41:184–90.
15. Vartanian RK, Weidner N. Correlation of intratumoral endothelial cell proliferation with microvessel density (tumor angiogenesis) and tumor cell proliferation in breast carcinoma. Am J Pathol 1994;144:1188–94.
16. McCarty KS, Jr., Miller LS, Cox EB, et al. Estrogen receptor analyses. Correlation of biochemical and immunohistochemical methods using monoclonal antireceptor antibodies. Arch Pathol Lab Med 1985;109:716–21.
17. Fidler IJ. Angiogenesis and cancer metastasis. Cancer J 2000;6:134–41.
18. Eliceiri B, Cheresh DA. The role of α_v integrins during angiogenesis: insights into potential mechanisms of action and clinical development. J Clin Invest 1999;103:1227–30.
19. Bello F, Francolini M, Marthyn P, et al. $\alpha(v)\beta3$ and $\alpha(v)\beta5$ integrin expression in glioma periphery. Neurosurgery 2001;49:380–9.
20. Brooks PC, Montgomery AM, Rosenfeld M, et al. Integrin $\alpha_v\beta_3$ antagonists promote tumor regression by inducing apoptosis of angiogenic blood vessels. Cell 1994;79:1157–64.
21. Wilder RL. Integrin $\alpha_v\beta_3$ as a target for treatment of rheumatoid arthritis and related rheumatic diseases. Ann Rheum Dis 2002;61 Suppl 2:96–9.
22. Pichler BJ, Kneilling M, Haubner R, et al. Imaging of delayed-type hypersensitivity reaction by PET and ^{18}F-galacto-RGD. J Nucl Med 2005;46:184–9.
23. Nip J, Shibata H, Loskutoff DJ, et al. Human melanoma cells derived from lymphatic metastases use integrin $\alpha_v\beta_3$ to adhere to lymph node vitronectin. J Clin Invest 1992;90:1406–13.
24. Felding-Habermann B. Integrin adhesion receptors in tumor metastasis. Clin Exp Metastasis 2003;20:203–13.
25. Felding-Habermann B, O'Toole TE, Smith JW, et al. Integrin activation controls metastasis in human breast cancer. Proc Natl Acad Sci U S A 2001;98:1853–8.
26. Byzova TV, Kim W, Midura RJ, et al. Activation of integrin $\alpha_v\beta_3$ regulates cell adhesion and migration to bone sialoprotein. Exp Cell Res 2000;254:299–308.
27. Stupack DG, Cheresh DA. A bit-role for integrins in apoptosis. Nat Cell Biol 2004;6:388–9.
28. Gasparini G, Brooks PC, Biganzoli E, et al. Vascular integrin $\alpha_v\beta_3$: a new prognostic indicator in breast cancer. Clin Cancer Res 1998;4:2625–34.
29. Vonlaufen A, Wiedle G, Borisch B, et al. Integrin $\alpha_v\beta_3$ expression in colon carcinoma correlates with survival. Mod Pathol 2001;14:1126–32.
30. McDonald DM, Choyke PL. Imaging of angiogenesis: from microscope to clinic. Nat Med 2003;9:713–25.
31. Raguse JD, Bath HJ, Bier J, et al. Cilengitide (EMD 121974) arrests the growth of a heavily pretreated highly vascularized head and neck tumor. Oral Oncol 2004;40:228–30.
32. Bilous M, Ades C, Armes J, et al. Predicting the HER2 status of breast cancer from basic histopathology data: an analysis of 1500 breast cancers as part of the HER2000 International Study. Breast 2003;12:92–8.